Self-Adaptive Fault-Tolerant Control of Three-Phase Series-End Winding Motor Drive

Xiangwen Sun, *Student Member, IEEE*, Zicheng Liu, *Member, IEEE*, An Li, *Member, IEEE*, Zhenyu Wang, Dong Jiang, and Ronghai Qu, *Fellow, IEEE*

***Abstract*—This article proposes a simplified fault-tolerant control (FTC) method for three-phase series-end winding motor drive, which has four bridges to achieve high voltage utilization and increased degrees of control freedom. Seven fault types are analyzed and the corresponding voltage/current derating is calculated. The proposed self-adaptive fault-tolerant strategy applied for the first fault category acts in both healthy and faulty conditions, which avoids the risk of delay and error caused by fault diagnosis, and achieves smooth fault-tolerant transition. Compared with existing FTC methods for the same structure, the proposed control strategy can achieve obviously better voltage utilization. In addition, to further exploit the maximum speed potential in the linear modulation zone, the improved common-mode voltage injection is adopted. The performance of the proposed fault-tolerant method is validated experimentally in an open-end three-phase induction machine system with the open-circuit fault.**

***Index Terms*—Fault tolerant control, induction motors, inverters, motor drives.**

I. Introduction

AS ELECTRICAL drive motors are employed in more and more important occasions [1], [2], reliability becomes a core index for evaluating system performance. However, the variable speed drive techniques relying on power electronics components increase the risks of faults in motor drive. Compared with multiphase motors, which can withstand multiple failures and possess the basis for passive fault tolerance due to inherent redundant control freedoms [3]–[5], [29], the three-phase motors with weak reliability still dominate the market share in most applications. Consequently, enough attention should be given to the fault-tolerant control (FTC) of the three-phase motor system.

There are two typical types of FTC for the three-phase system. The first type is the three-phase working mode, which means that all the three-phase windings can still work after the converter fault occurs. It can be achieved by alternate bridges or drive reconfiguration [6], [7], [25]. Although currents flow in all the windings, the maximum fault-tolerant output power might be decreased considering voltage and current limits of the inverter, unless the alternate bridge is implemented to ensure the unchanged drive structure before and after the faults [8]. The second type is the more prevalent two-phase working mode, in which the control complexity is increased compared with the three-phase mode [27]. To generate smooth torque, two remaining phase currents need to be adjusted in the magnitude and phase position to synthesize steady circular magnetomotive force (MMF) [9], [10]; hence, the zero-sequence current pathway is required for the newly created zero-sequence current components.

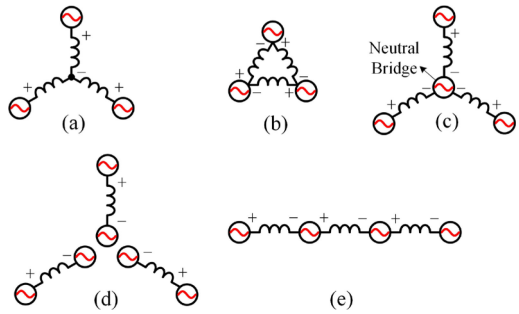

Fig. 1. Series of three-phase drive topologies. (a) Half bridge. (b) Delta type. (c) Three-phase four-leg. (d) Full bridge. (e) Series-end winding.

Based on the two-phase working principle above, a series of three-phase motor drive topologies with fault tolerance has been studied [11], [12]. Since the short-circuit faults [30] can be transformed into the open-circuit fault through the fuses, most of the research is based on the FTC of open phase/open circuit in the bridge. Traditional three-phase half bridge [shown in Fig. 1(a)] has poor fault-tolerant ability due to no zero-sequence current pathway. The delta topology owns the zero-sequence pathway with three bridges [see Fig. 1(b)]. However, this structure cannot generate circular MMF when the open circuit happens on any bridge, so the reliability is limited [13], [14]. The three-phase four-leg type with added neutral bridge, shown in Fig. 1(c), is proven with comprehensive fault-tolerant capability, but the large current capacity for the neutral bridge makes it not so attractive, especially on large-current occasions [15], [16]. The three-phase full-bridge type, shown in Fig. 1(d), owns the highest reliability because of decoupled winding voltage with two-side control freedom. Nevertheless, the high hardware expenses hinder the applications of full-bridge type in cost-sensitive areas.

Manuscript received December 12, 2021; revised February 23, 2022; accepted March 10, 2022. Date of publication March 22, 2022; date of current version May 23, 2022. This work was supported by the National Natural Science Foundation of China under Grants 51877091 and 52077088. Recommended for publication by Associate Editor J. Hur. *(Corresponding author: Zicheng Liu.)*

The authors are with the Huazhong University of Science and Technology, Wuhan 430074, China (e-mail: sunxw@hust.edu.cn; liuzc@hust.edu.cn; anli@hust.edu.cn; wang_zhenyu@hust.edu.cn; jiangd@hust.edu.cn; ronghaiqu@hust.edu.cn).

Color versions of one or more figures in this article are available at https://doi.org/10.1109/TPEL.2022.3160747.

Digital Object Identifier 10.1109/TPEL.2022.3160747

The topology determines whether the system has fault tolerance capability. The corresponding FTC methods are related to the postfault performance, mainly in transient procedure and output capacity. After the fault occurs, the system may be in an unstable state during the fault diagnosis time. The self-adaptive operation can help the system skip this stage and switch quickly to the fault-tolerant algorithm, which is realized in experiments with full-bridge and delta type [7], [14]. However, the theoretical basis for self-adaptive FTC has not been analyzed to explore the implementation principle.

Because the remaining phase currents need to be increased to keep unchanged MMF in two-phase working mode, the current output capacity inevitably declines after the fault occurs. The postfault output capacity is mainly determined by voltage utilization. However, even for the full-bridge topology with the highest voltage utilization in healthy conditions, the existing methods cannot further retain the important advantage with whether open-phase fault [10] or open-circuit in bridge [19]. Although more bridges are used, the output performance has not been effectively improved.

As shown in Fig. 1(e), the series-end winding motor drive (SWMD) topology has three-phase windings connected in series, and four accessible nodes connected to four inverter legs, respectively. It has been proved to own good performance like the same high voltage utilization as the full-bridge topology and zero-sequence controllability with only one more bridge [17], [18]. Because the number of bridges is one more than that of the windings, the reliability and control freedom of SWMD is worth discussing.

This article proposes a self-adaptive FTC method used in three-phase SWMD, which realizes the fault tolerance of SWMD for the first time. The theoretical derivation and control principle of the self-adaptive mechanism is also introduced in detail. From prefault to postfault conditions, the control method remains unchanged to avoid the oscillations caused by the transition of control, which effectively reduces the requirement for quick fault diagnosis. After the fault, the maximum operation speed/power with the proposed FTC method has obvious advantages over existing space-vector (SV) methods [19], [24]. Combined with the common-mode voltage (CMV) injection, the fault-tolerant operation speed range can be further extended.

The rest of the article is organized as follows. The mathematical analysis of a healthy drive system is presented in Section II. Then, the postfault motor and topology characteristics are introduced in Section III. In Section IV, the self-adaptive FTC scheme of three-phase SWMD is proposed, containing the field-oriented control strategy and the improved CMV injection method. Experimental setup and results in Section V verify the effectiveness of the proposed FTC method. Finally, Section VI concludes this article.

II. Healthy Drive System

The healthy three-phase SWMD is shown in Fig. 2. Different from traditional topologies in which the winding voltage equals the corresponding bridge output, the voltage of each phase winding is determined by two bridge outputs at its ends in the

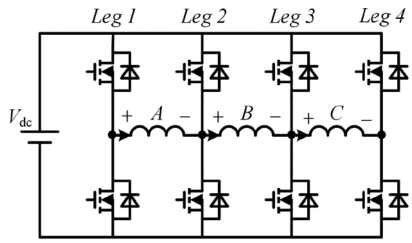

Fig. 2. Three-phase series-end winding topology.

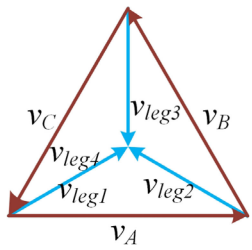

Fig. 3. Vector relationship between the phase voltage and bridge voltage.

following equation:

$$\begin{bmatrix} v_A \\ v_B \\ v_C \end{bmatrix} = \begin{bmatrix} 1 & -1 & 0 & 0 \\ 0 & 1 & -1 & 0 \\ 0 & 0 & 1 & -1 \end{bmatrix} \begin{bmatrix} v_{\text{leg1}} \\ v_{\text{leg2}} \\ v_{\text{leg3}} \\ v_{\text{leg4}} \end{bmatrix} \tag{1}$$

where v_A–v_C are the phase winding voltages and v_{leg1}– v_{leg4} are output voltages of inverter bridges. Based on the general pulsewidth modulation (PWM) method [18], the bridge modulation wave can be obtained through phase voltage

$$\begin{bmatrix} V_{\text{ld}}(m) \\ V_{\text{lq}}(m) \end{bmatrix} = \frac{1}{2} \begin{bmatrix} 1 & \cot\frac{\alpha}{2} \\ -\cot\frac{\alpha}{2} & 1 \end{bmatrix} \begin{bmatrix} V_{\text{d}}(m) \\ V_{\text{q}}(m) \end{bmatrix} \tag{2}$$

where V_{ld} and V_{lq} are the leg voltage components in the rotating frame, and V_{d} and V_{q} are the stator voltage components in the rotating frame. $\alpha = 2\pi/3$. It should be noted that the positive and negative sequences need to be transformed separately by (2), and the m represents the rotation direction in which $m = 1$ means positive sequence and $m = -1$ means negative sequence.

The voltage utilization represents the maximum voltage that can be obtained in phase winding, which directly determines the operating speed range of the motor at a fixed dc-link voltage. The voltage utilization is defined as the maximum phase voltage magnitude divided by the V_{dc}. For example, the voltage utilization of Fig. 1(a) is 0.5 without min-max injection, which could be 0.577 with injection.

Based on the above modulation method, the corresponding voltage vector diagram for SWMD is shown in Fig. 3, and the voltage utilization is $\sqrt{3}$ times that of the half-bridge structure. With the same dc-link voltage, SWMD can significantly increase the speed range of the motor. Because of this advantage, SWMD becomes a good candidate for many areas including traction and propulsion. Its structure for FTC is also with merit, which is discussed in this article for the first time.

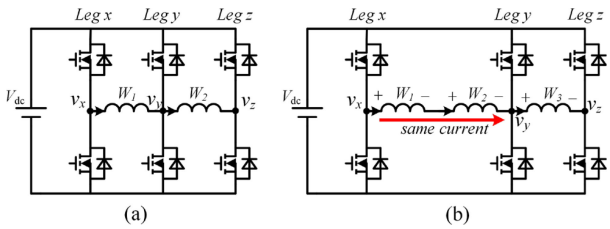

Fig. 4. Postfault drive structure. (a) Category 1: the failure of leg1, leg4, or phase windings. (b) Category 2: the failure of leg2/leg3.

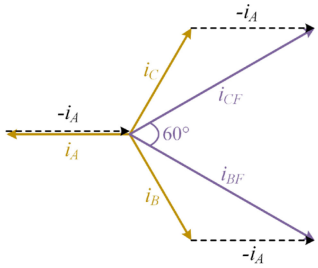

Fig. 5. Current distribution after open circuit occurs on phase *A*.

It should be noted that the current stress of center bridges leg2 and leg3 is $\sqrt{3}$ times that of winding current. The SWMD can be seen as a special case in a full-bridge topology with a 120° phase-shift between two-side inverters, where two bridges are multiplexed as center bridges to reserve high voltage utilization and zero-sequence controllability. So the multiplexed bridges are required to bear the line current rather than phase current.

III. Faulted Drive System

A. Fault Condition Analysis

It should be noted that the faults mentioned in this article are all open-circuit faults. There are totally seven typical failure conditions, including four bridge failures (leg1–leg4) and three winding failures (phases *A*–*C*). Different from most of the centrosymmetric topology, the current restriction brought by inverter failure is not completely equivalent to that by winding failure in SWMD. According to the postfault drive structure, the seven failure conditions can be divided into two categories.

The first category involves the failures of leg1, leg4, or phase windings, which leads to the zero current of the corresponding phase, whereas the other two-phase currents are not influenced. The postfault drive operates similarly to the "two-phase series-end winding" topology, as shown in Fig. 4(a). When the fault occurs on phase *B*, the postfault structure is equivalent to the full-bridge topology with a single-phase fault [10]. It can also be seen as a special case where two middle legs [leg *y* in Fig. 4(a)] are used to drive windings W_1 and W_2, respectively.

An important criterion to prove the fault tolerance is that the unchanged MMF can be synthesized under the failure constraint. The MMF in healthy and faulty conditions is given in (3). Before the fault, the windings are flowed through symmetrical three-phase current $i_A = I_{\mathrm{m}}\cos(\omega t)$, $i_B = I_{\mathrm{m}}\cos(\omega t – 2\pi/3)$, $i_C = I_{\mathrm{m}}\cos(\omega t – 4\pi/3)$. After the fault (take the failure of phase A as an example), i_A is restricted to zero. The new effective current solution that meets constant MMF in the first category of fault can be found in (4)

$$\begin{aligned}\mathrm{MMF}_H &= i_A\cos\theta + i_B\cos\left(\theta-\frac{2}{3}\pi\right) + i_C\cos\left(\theta-\frac{4}{3}\pi\right)\\ \mathrm{MMF}_H &= i_{BF}\cos\left(\theta-\frac{2}{3}\pi\right) + i_F\cos\left(\theta-\frac{4}{3}\pi\right) \qquad (3)\\ \mathrm{MMF}_H &= \mathrm{MMF}_F\end{aligned}$$

$$i_{AF} = i_A - i_A = 0, i_{BF} = i_B - i_A, i_{CF} = i_C - i_A. \qquad (4)$$

From the results, we can find that the postfault current distribution equals the healthy three-phase currents with superposition of a common zero-sequence component that is opposite to the faulty phase, as depicted in Fig. 5. The phase difference of two-phase currents changes from 120° to 60° and the magnitude should be increased by a factor of $\sqrt{3}$. Therefore, under the first category of fault, the SWMD can achieve fault-tolerant operation in two-phase mode, at the expense of decreasing output capacity.

The second category represents the failure of leg2 or leg3, which means two windings flow through the same currents, as shown in Fig. 4(b). In this restriction, the winding connection mode used in the article cannot satisfy (3) to synthesize a circular MMF to generate smooth torque. Once the kind of fault occurs, the motor can only be stopped. Hence, the bidirectional thyristors are necessary for the faults of category 2 to perform reconfiguration to obtain an identical structure as the first category [19], [20]. Unstable transition cannot be avoided in this fault and a different FTC method from that in category 1 is needed to solve this type of fault.

It can be concluded that three-phase SWMD can withstand five fault conditions without any hardware assistance and two fault conditions with hardware reconfiguration, showing strong reliability over most three-phase topologies. Although the second category of fault could be converted to the first category through reconfiguration, a completely different FTC procedure is needed to solve the second category (like fault diagnosis requirement, hardware, and modulation). In this article, we focus on the control of the first category that contains more types of faults in Fig. 4(a). Considering that the fault diagnosis methods are independent topics and have been addressed in publications [21]–[23], the detailed fault diagnosis will not be concerned and discussed in this article.

B. Postfault Control Characteristics

Section III-A proves that the motor can achieve fault-tolerant operation with smooth torque output under the first category of fault. In this section, the purpose is to discuss how to control the topology to ensure that the aforementioned modified phase currents can be realized.

It should be noted that whether it is an open circuit of winding or leg, the fault can be seen as a high-resistance resistor R_∞ connected in series with the corresponding phase winding, shown in Fig. 6, which will help calculate the two-phase model from the three-phase perspective. The SWMD owes characteristics

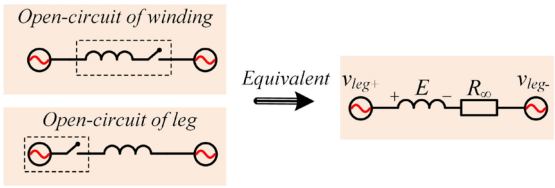

Fig. 6. The equivalent schematic of open-circuit fault.

similar to the full-bridge topology in which the stator voltage of each phase is fully decoupled and only determined by the output of the leg. Consequently, take resistance R_s and leakage inductance L_σ as stator impedance $Z_s = (R_s + j\omega L_\sigma) \ll R_\infty$ we can get postfault voltage and current relationship (A-phase fault as an example)

$$\begin{aligned} &\boldsymbol{v}_{abc} = [\boldsymbol{R}]\boldsymbol{i}_{bc} + \boldsymbol{E}_{abc} \\ \Rightarrow &\begin{bmatrix} v_A \\ v_B \\ v_C \end{bmatrix} = \begin{bmatrix} R_\infty + Z_s & 0 & 0 \\ 0 & Z_s & 0 \\ 0 & 0 & Z_s \end{bmatrix} \begin{bmatrix} i_A \\ i_B \\ i_C \end{bmatrix} + \begin{bmatrix} E_A \\ E_B \\ E_C \end{bmatrix} \end{aligned} \tag{5}$$

where $\boldsymbol{E}_{abc}$ means electromotive force (EMF), and $\boldsymbol{R}$ means postfault three-phase stator impedance. To get the zero-sequence information, the rotation transformation matrix T through constant power conversion (identical to traditional three-phase transformation matrix) is introduced

$$\begin{aligned} &\boldsymbol{v}_{dq0} = T[\boldsymbol{R}]T^{-1}T\boldsymbol{i}_{abc} + \boldsymbol{E}_{dq0} \\ &T = \sqrt{\frac{2}{3}} \begin{bmatrix} \cos\theta & \cos(\theta - \frac{2}{3}\pi) & \cos(\theta - \frac{4}{3}\pi) \\ -\sin\theta & -\sin(\theta - \frac{2}{3}\pi) & -\sin(\theta - \frac{4}{3}\pi) \\ \sqrt{\frac{1}{2}} & \sqrt{\frac{1}{2}} & \sqrt{\frac{1}{2}} \end{bmatrix}. \end{aligned} \tag{6}$$

After the substitution and calculation, the voltage and current relationships in $dq0$-plane can be obtained in the following equation:

Because the zero-sequence voltage of fundamental frequency for the windings is not injected in the healthy condition, $v_0 = 0$

$$\begin{aligned} 0 = v_0 &= \frac{2}{3}R_\infty \left(\frac{1}{\sqrt{2}} \cos\omega t \cdot i_d - \frac{1}{\sqrt{2}} \sin\omega t \cdot i_q + \frac{1}{2} i_0 \right) + Z_s i_0 \\ \Rightarrow\ &-\frac{3}{2}\frac{Z_s i_0}{R_\infty} = \frac{1}{\sqrt{2}} \cos\omega t \cdot i_d - \frac{1}{\sqrt{2}} \sin\omega t \cdot i_q + \frac{1}{2} i_0 \approx 0 \\ \Rightarrow\ &i_0 = \sqrt{2} \sin\omega t \cdot i_q - \sqrt{2} \cos\omega t \cdot i_d = \frac{1}{\sqrt{3}}(i_a + i_b + i_e) \\ \Rightarrow\ &\sqrt{\frac{1}{3}} i_0 = -i_a. \end{aligned} \tag{8}$$

This means that the zero-sequence current is identical to the restriction in (4). It can be easily found that even without zero-sequence voltage control of fundamental frequency, the natural phase current distribution due to the open-circuit fault can satisfy the fault-tolerant operation requirements in (3) (considering the symmetry, other phase failures have the same conclusion), which provides a theoretical basis for simplified FTC. The full-bridge topology owes characteristics similar to SWMD in which the stator voltage of each phase is fully decoupled; hence, the work in [7] utilized the same fault tolerance foundation to achieve smooth FTC with full-bridge structure through SVPWM.

For a faulty motor, the most important task is to be able to withstand the impact of failure, which represents fault tolerance. The second most important is the postfault voltage/current output capacity (derating), which represents the significance of fault tolerance.

Actually, the derating discussed here is always related to the motor rather than the power converter, since the design of the converter generally has sufficient margin for the consideration of FTC or long lifetime. As for the limitation of motor, we take the rated parameter of motor (rated voltage and phase current) as 100% operation performance upper limit to ensure insulation safety (voltage) and heat safety (current).

For the postfault current output capacity, the postfault phase current magnitude is increased by a factor of $\sqrt{3}$ to keep constant MMF. Hence, $1/\sqrt{3}$ of maximum current component that contributes flux and torque can be reached when the windings flow through the currents of the rated amplitude. In some special occasions like flux weakening of permanent magnet synchronous motor (PMSM), the torque derating varies in a certain degree [26].

For the voltage, the derating is related to voltage utilization due to the fixed dc-link voltage on most occasions. Changed postfault topology may greatly influence the magnitude of the phase voltage with an unchanged modulation index [28]. The inverter output in the dq-axis equals the EMF in dq-axis when neglecting the voltage drop on the R_s and L_σ. After the fault, the decrease of voltage utilization is related to the variation of the high-resistance items in (6) and (7) shown at the bottom of this page. Substitute (8) into the $T[\boldsymbol{R}]T^{-1}\boldsymbol{i}_{dq0}$ term

$$\begin{aligned} \Delta v_d &= \frac{2}{3}R_\infty \left(\cos^2\omega t \cdot i_d - \sin\omega t \cos\omega t \cdot i_q \right. \\ &\qquad \left. + \frac{1}{\sqrt{2}} \cos\omega t \cdot i_0 \right) = 0 \\ \Delta v_q &= \frac{2}{3}R_\infty \left(-\sin\omega t \cos\omega t \cdot i_d \right. \\ &\qquad \left. + \sin^2\omega t \cdot i_q - \frac{1}{\sqrt{2}} \sin\omega t \cdot i_0 \right) = 0. \end{aligned} \tag{9}$$

$$\begin{bmatrix} v_d \\ v_q \\ v_0 \end{bmatrix} = \frac{2}{3} \begin{bmatrix} R_\infty \cos^2\omega t + \frac{3}{2}Z_s & -R_\infty \sin\omega t \cos\omega t & \frac{1}{\sqrt{2}}R_\infty \cos\omega t \\ -R_\infty \sin\omega t \cos\omega t & R_\infty \sin^2\omega t + \frac{3}{2}Z_s & \frac{-1}{\sqrt{2}}R_\infty \sin\omega t \\ \frac{1}{\sqrt{2}}R_\infty \cos\omega t & \frac{-1}{\sqrt{2}}R_\infty \sin\omega t & \frac{1}{2}R_\infty + \frac{3}{2}Z_s \end{bmatrix} \begin{bmatrix} i_d \\ i_q \\ i_0 \end{bmatrix} + \begin{bmatrix} E_d \\ E_q \\ E_0 \end{bmatrix}. \tag{7}$$

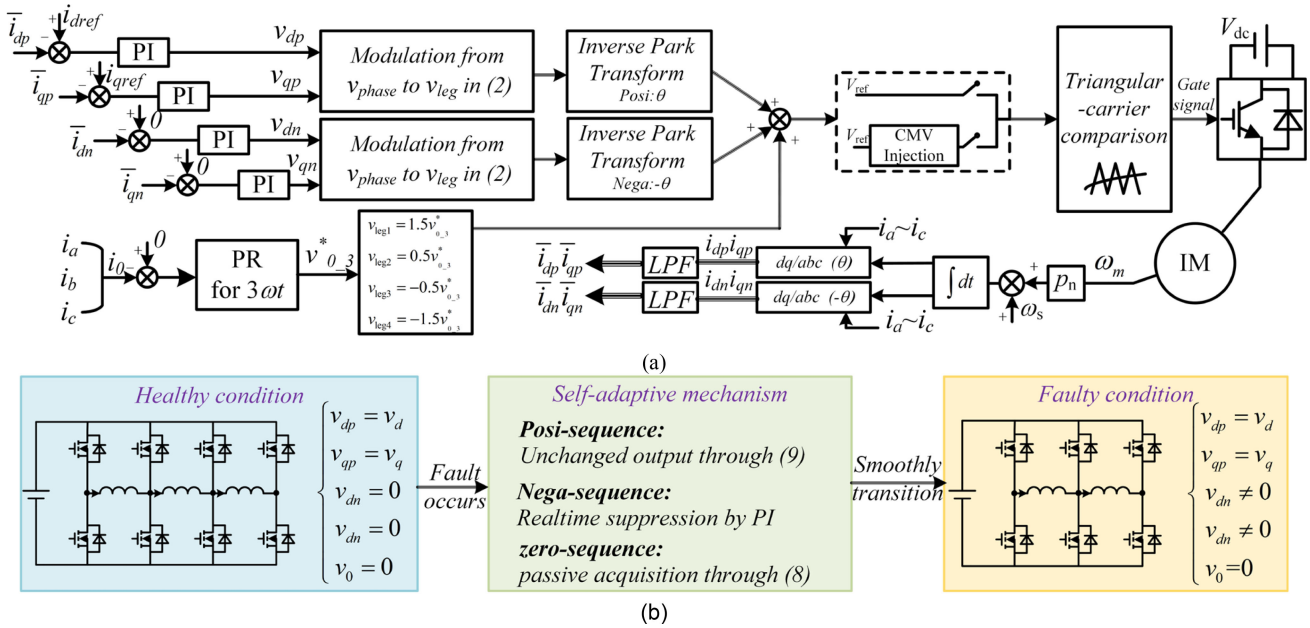

Fig. 7. Proposed control method for three-phase SWMD with the self-adaptive capability. (a) Control diagram. (b) Self-adaptive mechanism.

We can clearly conclude that the voltage utilization is constant before and after fault since no more *dq*-axis voltage is required to inject for postfault topology. Combined with high voltage utilization in healthy condition, the SWMD is quite suitable for scenarios where the high speed and reliability is extremely urgent.

Based on the current/voltage capacity analysis above, the current is the only limit for a postfault motor system. The calculated maximum output power is $1/\sqrt{3}$ of rated power in general cases.

It should be noted that the actual derating of voltage utilization is slightly larger than the theoretical value above due to the fault-induced impedance asymmetry, which is discussed in detail in the following section.

IV. Self-Adaptive FTC Method for Three-Phase SWMD

The whole control scheme of the proposed field-oriented FTC method applied for the first category of fault is shown in Fig. 7. Compared to the traditional motor control strategy, some extra techniques for postfault performance improvement are adopted in the FTC method.

A. Negative-Sequence Suppression

In healthy conditions, the windings are with symmetrical impedance. Even considering the voltage drop of the leakage impedance, the stator voltages are still symmetrical, as shown in Fig. 8(a), in which $\omega L_\sigma \ll R_s$ for simplification. The inverter can output symmetrical voltages to obtain desired three-phase currents. However, after the fault occurs, the impedance of the postfault controlled motor is no longer symmetrical through the analysis of the three-phase perspective. Based on the calculated new current distribution, we can get postfault stator voltage distribution with unequal magnitude and phase shift, as shown

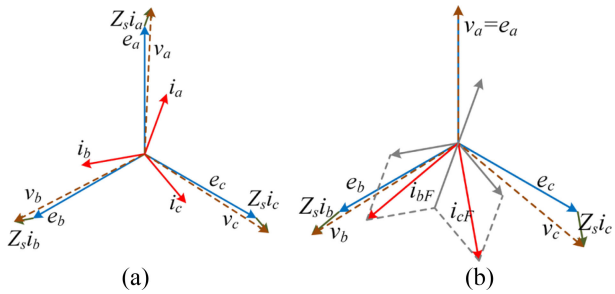

Fig. 8. Stator voltage vector diagram. (a) Before the fault. (b) After the Phase-*A* fault.

in Fig. 8(b). If the inverter still outputs normal voltage under faulty condition, there will be asymmetrical phase currents, which could be decomposed into positive-, negative-, and zero-sequence current components. The positive sequence contributes to the flux and torque, and the fundamental-frequency zero-sequence current helps to synthesize unchanged postfault MMF. But the negative-sequence component produces the MMF that rotates opposite to the positive sequence and generates torque ripple. To intuitively prove the harm caused by the negative sequence, we could assume

$$\begin{aligned} I_a &= k_+\cos(\omega t) + k_-\cos(-\omega t) + k_0 \\ I_b &= k_+\cos\left(\omega t - \frac{2}{3}\pi\right) + k_-\cos\left(-\omega t - \frac{2}{3}\pi\right) + k_0 \\ I_c &= k_+\cos\left(\omega t - \frac{4}{3}\pi\right) + k_-\cos\left(-\omega t - \frac{4}{3}\pi\right) + k_0. \end{aligned} \quad (10)$$

Equation (10) can represent phase current distribution in any condition, and k_+, k_-, and k_0 mean positive, negative, and zero sequence. When the k_- is nonzero, we could use transformation

in (6) to get corresponding *dq*-plane component like (where $\theta = \omega t + \varphi$)

$$\begin{aligned} I_{dp} &= \sqrt{\frac{3}{2}}k_+ \cos(\theta - \omega t) + \sqrt{\frac{3}{2}}k_- \cos(\theta + \omega t) \\ &= \sqrt{\frac{3}{2}}k_+ \cos(\varphi) + \sqrt{\frac{3}{2}}k_- \cos(2\omega t + \varphi) \\ &= \mathrm{cons\,tant} + \sqrt{\frac{3}{2}}\mathrm{k}_- \cos(2\omega \mathrm{t} + \varphi). \end{aligned} \tag{11}$$

Similar results can also be found in the *q*-axis current (subscript *p* means the transformation is based on the rotation direction of ωt). Since the output torque $T \propto i_{dp} \cdot i_{qp}$, the existence of negative sequence would cause useless low-frequency torque ripple and extra winding losses. For the SWMD, the fault-induced negative sequence is mainly caused by the leakage impedance Z_s in Fig. 8(b); the suppression of the negative-sequence component can effectively improve the postfault torque quality.

In the proposed current control method for SWMD, in addition to the basic control for positive-sequence component including flux (i_{dp}) and torque (i_{qp}), the negative-sequence (i_{dn}, i_{qn}) proportional-integral (PI) controllers are also added regardless of whether the fault occurs. In healthy conditions, almost no negative-sequence current can be measured due to highly symmetrical three-phase winding; the corresponding negative-sequence PI controller output voltage is nearly zero. After the fault occurs, the winding symmetry is broken, and then the considerable negative-sequence currents appear as the harmonics in i_{dp}, i_{qp}, which cause low-order torque pulsations and additional losses. The negative-sequence PI controller (i_{dn}, i_{qn}) can effectively suppress the negative-sequence current, which is mainly reflected as dc components in negative-sequence rotation transformation (rotation direction of $-\omega t$), and thus suppress the torque pulsations. Meanwhile, the fundamental-frequency positive-sequence currents reflect as twice-fundamental-frequency components for the negative-sequence controllers, and therefore are not obviously affected due to the low bandwidth of negative-sequence PI controllers. In low-speed operation, the negative-sequence PI controllers with low output limitation would not affect the system stability.

It should be noted that the impedance of the nonpositive-sequence plane is so low that the voltage utilization drop by negative-sequence suppression is limited, which will be revealed in experimental results. Moreover, the adopted Park [shown in (6)] and inverse Park transformation matrix is identical to the traditional transformation matrix, and they are unchanged before and after the fault.

B. Zero-Sequence Harmonic Suppression

The acquisition of the zero-sequence pathway not only ensures the SWMD gain satisfying fault-tolerant basis but also allows all types of zero-sequence components to flow. Concerning there is obvious zero-sequence component of three times the fundamental frequency in the EMF of actual motors, and other nonideal factors like deadtime, system asymmetry, the specific proportional-resonant (PR) controller is adopted to suppress the unwanted component, no matter in healthy or any faulty conditions. The zero-sequence can be calculated through the third row of the matrix (6). The PR controller is applied to control only the triple frequency component that is set to resonant frequency point. Since the gain of the PR controller at the nonresonant frequency is very low, the components at the nonresonant frequency will not be influenced by it. The zero-sequence voltage distribution method in bridge output adopts the method in [18], which has been given in Fig. 7.

It is worth distinguishing that the zero-sequence suppression here only focuses on the components of three times the fundamental frequency $3\omega t$, resulting from the nonideal motor EMF. However, the zero-sequence current discussed in Section III-B, which appears after the fault to achieve fault tolerance is at the fundamental frequency ωt. Moreover, the nonideal zero-sequence component can also affect the voltage utilization at a limited level, which is neglected in the theory analysis and presented in experiments.

C. CMV Injection-Increased Linear Speed Range Limit

To fully exploit the voltage utilization limit, the improved CMV injection can be adopted. Different from the zero-sequence component that corresponds to the identical part of motor phase windings, the common-mode component is the CMV of the inverter bridges, which will not influence the phase winding voltage since the winding voltage is the difference of the two-side inverter-bridge voltages. In healthy condition, we have

$$\begin{aligned} v_{\mathrm{com}} &= -\frac{1}{2}(v_{\max} + v_{\min}) \\ v_{\max} &= \max\{v_{\mathrm{leg1}} \sim v_{\mathrm{leg4}}\} \\ v_{\min} &= \min\{v_{\mathrm{leg1}} \sim v_{\mathrm{leg4}}\}. \end{aligned} \tag{12}$$

The max/min function is to find the maximum/minimum value among several references in the brackets.

Considering that there is a zero-sequence control (for components of $3\omega t$), the modulation waves of v_{leg1} and v_{leg4}, which should be equal in theory (depicted in Fig. 4), are inconsistent. When the postfault two-phase structure applies the CMV injection above, it is better to strip off the wave of the faulty bridge in (12) to get postfault optimal CMV-injection results.

D. Design and Realization of Motor Control

To improve the system stability, the speed-loop bandwidth is designed much lower than the current loop. Meanwhile, the speed information sample (from the encoder) is with a common low-pass filter to suppress the unwanted disturbance.

As for the induction motor, the slip frequency ω_s should be calculated through

$$\omega_s = \frac{L_m {i_{qp}}^*}{\tau_r {\psi_{rd}}^*} \tag{13}$$

where $\tau_r = L_r/R_r$, ${i_{qp}}^*$ means the *q*-axis current reference, and ${\psi_{rd}}^*$ means the rotor flux reference. Combined with the speed

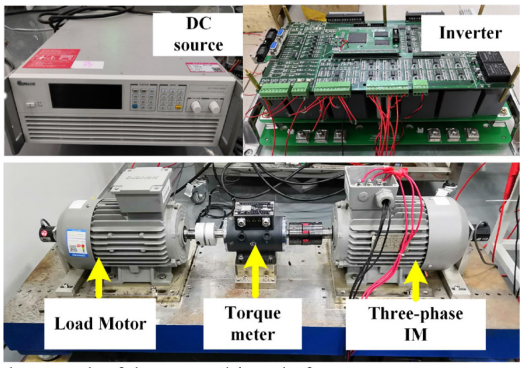

Fig. 9. Photograph of the motor drive platform.

information from the encoder (measure the mechanical speed ω_m), the rotor flux angle can be obtained.

To track the current references, the inverter phase leg output voltages should be obtained through PI controllers. According to (1), for the three-phase SWMD, the phase winding voltage is not equal to the bridge voltage; the modulation that converts the winding voltage to the two-side bridge voltage is needed. Afterward, the modulation wave in the *dq*-axis should be transformed to reference waves in the *abc*-axis by the traditional inverse transformation matrix. The thing that needs to be noted is that positive sequence uses θ and the negative sequence uses $-\theta$, as shown in Fig. 7.

We choose SPWM rather than SVPWM to eliminate the need for switching state analysis and get a better extension for more multiphase cases in future work.

E. Self-Adaptive Mechanism of the Method

The self-adaptive mechanism of the proposed FTC method is given in Fig. 7. The derivation results of (3)–(9) are the theoretical basis for realizing the self-adaptive control. After the fault occurs, the zero-sequence current is needed to keep the unchanged MMF. Fortunately, (8) shows that the zero-sequence components can be obtained naturally by postfault circuit structure, without dedicated zero-sequence control. Moreover, the voltage equation (9) shows that the positive sequence of phase voltage is kept unchanged. Consequently, the SWMD can achieve continued stable operation after the fault even without control assistance.

As stated in Section IV-A, the negative sequence appears after the fault and causes harmful torque ripple. However, the added PI controller can be activated before the fault, and actively suppress the negative-sequence component without fault diagnosis and location. So the proposed control strategy of the SWMD needs no control adjustment of the positive, negative, and zero-sequence. The system can smoothly transition from the healthy condition to faulty operation and achieve the self-adaptive FTC.

V. Experimental Validation

To validate the performance of the proposed FTC method for three-phase SWMD under the first category of fault, experiments were conducted on a three-phase induction motor platform under the *A*-phase fault (achieved by a breaker), as shown in Fig. 9, with a conventional three-phase IM fed by a commercial converter acting as the load. The general inverter is employed to feed the three-phase open-end winding induction machine, the general inverter is composed of two insulated gate bipolar transistor (IGBT) modules (FS100R12KT4G from Infineon, $V_{\text{cemax}} = 1200$ V, $I_N = 100$ A). The proposed control method has been implemented using a DSP TMS320F28377D controller board from Texas Instrument. The switching frequency is 10 kHz and the leg deadtime is set to 1 μs. The main parameters of the three-phase motor are listed in Table I.

TABLE I
Parameters of Induction Machine

Parameter	Value	Parameter	Value
Pole Pairs	1	Rated Power (kW)	2.2
Rated Voltage (V)	220	Rated Current (A)	4.75
Rated Speed (rpm)	2890	Stator Self-Inductance (mH)	269.2
Stator Resistance (Ω)	2.876	Stator Leakage Inductance (mH)	9.5

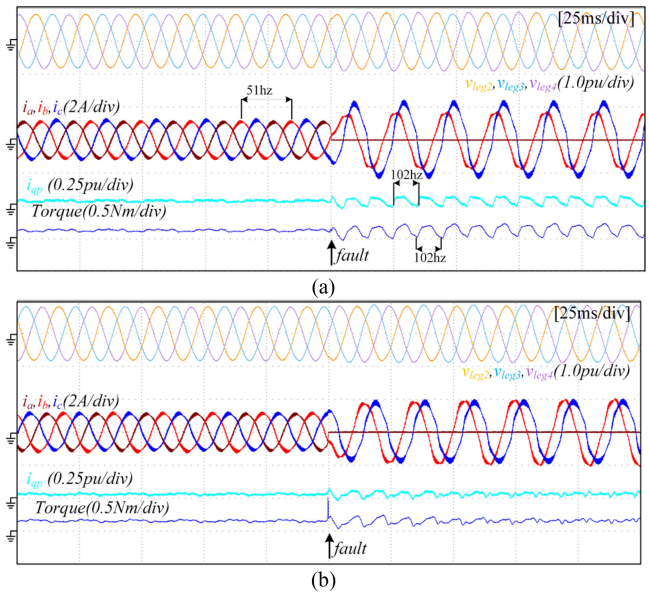

Fig. 10. Fault transient test result under light load. (a) Proposed FTC method without negative-sequence suppression. (b) Proposed FTC method with negative-sequence suppression.

To fully analyze the postfault characteristics of the topology and demonstrate the effectiveness of the proposed method, the experiments are carried out in fault transient procedure, dynamic performance, and voltage utilization test.

A. Fault Transient Procedure

The fault transient test under light load is carried out at the speed of 3000 r/min in Fig. 10. The fault is with i_a to be turned to zero by opening the breaker. The three-phase currents are given to show current distribution information, and the *q*-axis current from positive-sequence transformation can represent the output torque information (torque value and ripple). Before the fault occurs, the symmetrical three-phase currents and modulation waves represent that the motor is with

TABLE II
POSTFAULT PERFORMANCE COMPARISON WITH/WITHOUT NEGATIVE-SEQUENCE SUPPRESSION (SEE FIG. 10)

State	Healthy	Faulty	
		Before suppression	After suppression
Torque ripple / Nm	0.13 Nm	0.29 Nm	0.15 Nm
Current asymmetry ζ	8.4%	27.5%	8.8%

symmetrical impedance. The amplitude of the modulation wave is about 0.81 p.u. The q-axis current is with a high-frequency ripple of 0.03 p.u. peak-to-peak (p-p) value. The torque ripple is 0.13 N·m. Then, the current of phase A is clamped to zero by fault, the results show that the motor can effectively withstand the assault caused by open-circuit failure without fault diagnosis, and the maximum magnitude of modulation wave is increased only 10% to 0.89 p.u., which shows the high voltage utilization characteristics of three-phase SWMD.

Fig. 10(a) shows that the motor system can still work at rated speed after the fault even without negative suppression. However, considerable negative-sequence component can be captured from currents (imbalance between i_b and i_c, second-order harmonic with 0.1 p.u. p-p value in i_{qp}) and torque ripple of 0.29 N·m, which deteriorate the output performance and cause extra derating due to imbalanced current distribution.

To quantify the influence of current asymmetry caused by negative sequence, we define the current asymmetry ς

$$\zeta = \frac{|m_{\max}| - |m_{\min}|}{|m_{\max}|} \times 100\% \tag{14}$$

where $m_{\max}$ represents the amplitude of the current with maximum amplitude and $m_{\min}$ represents the amplitude of the current with minimum amplitude. ζ increases from 8.4% to 27.5% when the fault occurs without negative-sequence suppression. Hence, the negative-sequence component can cause obvious current imbalance and torque ripple under the light load.

If the negative-sequence suppression is activated in Fig. 10(b), the negative-sequence component is effectively suppressed in less than 100 ms. The p-p value of i_{qp} is less than 0.05 p.u. in steady state, the torque ripple is reduced to 0.15 N·m, and ζ is less than 9%, which is very close to a healthy value. Besides, the results show that the negative-sequence suppression will not interfere with the operation of the system in healthy condition, proving that the FTC method needs no adjustment or switching with the assistance of fault diagnosis, and achieve fast self-adaptive after the fault occurs. Moreover, the use of negative-sequence suppression will not influence voltage utilization through postfault modulation wave distribution results from Fig. 10(a) and (b). To intuitively reveal the effectiveness of the negative-sequence suppression, the quantified analysis is given in Table II.

To prove the proposed controller can achieve successful performance even with heavy load, a fault transient test under 50% of the rated load is given in Fig. 11(a). It should be noted that the load is set at about 50% of the rated value considering the postfault derating. From the results, we can find that the

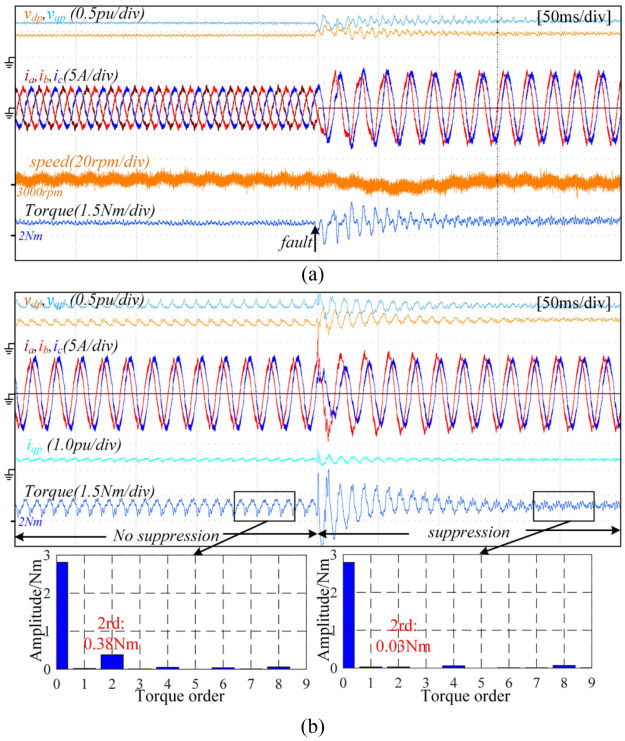

Fig. 11. Fault transient test result under 50% of rated load. (a) Proposed FTC method with negative-sequence suppression. (b) Torque ripple comparison without/with negative-sequence suppression.

fault tolerance is still excellent even in heavy load. After the fault occurs, the magnitude of the positive sequence remains almost unchanged, proving the correctness of (9). The speed oscillations caused by torque ripple are hard to be detected even in high-load conditions due to large rotation inertia. Fig. 11(b) shows the fast Fourier transform analysis comparison results of output torque without/with negative-sequence suppression. The double-frequency torque ripple can be reduced from 0.38 to 0.03 N·m after the negative-sequence suppression, and the postfault torque output quality can be greatly improved with the proposed control method.

To verify the feasibility of the proposed zero-sequence suppression method, a comparison test is given in Fig. 12. To prove the suppression effect under the most serious zero-sequence issue, the excitation current is set to a rated value under load. In healthy conditions, the currents without zero-sequence current (ZSC) suppression are like trapezoidal waves. By calculating the sum of currents $i_{\text{sum}} = i_a + i_b + i_c$, the triple frequency component with a p-p value of 4.03 A can be obtained. After activating the PR controller, the i_{sum} is reduced to 1.32 A, and the remaining part mainly comes from higher frequency ZSC such as sixth and ninth harmonics. The current quality is improved obviously. The zero-sequence component of bridge output is also given, showing agreement with theoretical analysis. In faulty conditions, the PR controller can also suppress the third harmonic without affecting the fault tolerance.

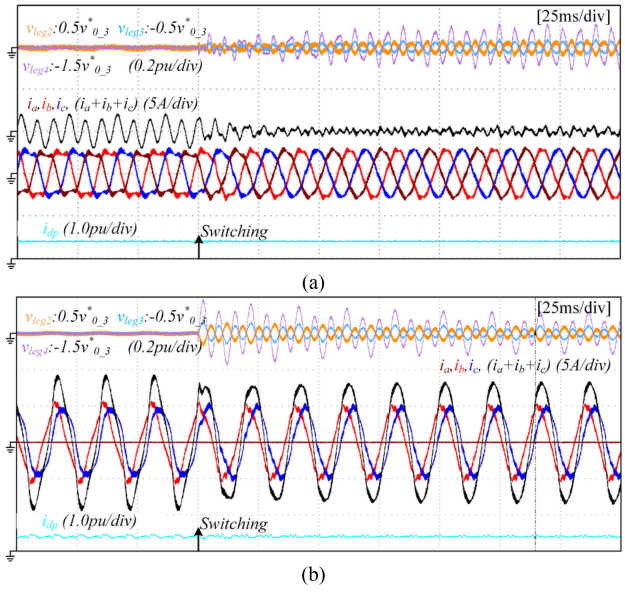

Fig. 12. Suppression comparison about the zero-sequence component of three times the fundamental frequency under: (a) healthy condition and (b) faulty condition.

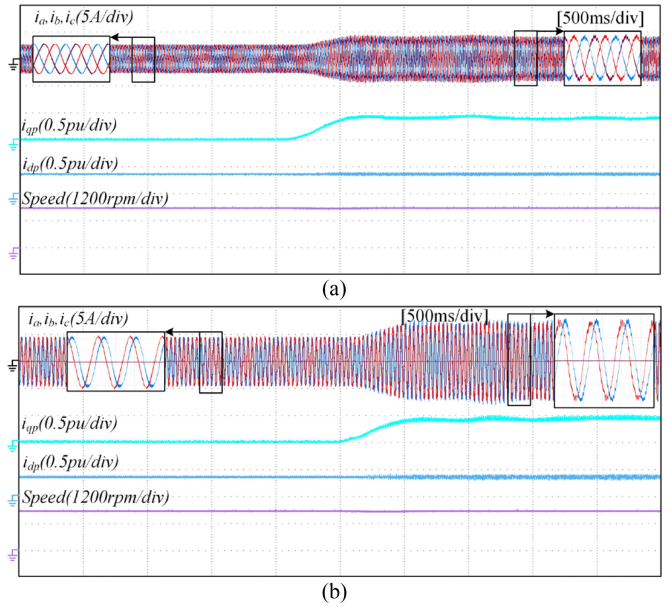

Fig. 14. Experimental results of load transient stability. (a) Healthy condition. (b) Faulty condition.

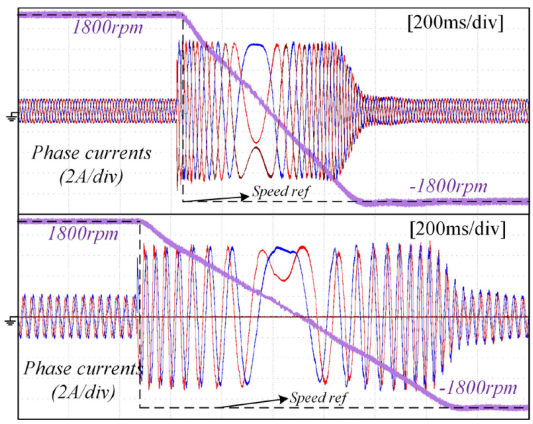

Fig. 13. Dynamic response comparison test of reversal rotation. Upper: healthy condition. Lower: postfault condition.

B. Dynamic Performance Test

The dynamic response test is executed in Fig. 13. The reference speed is stepped from 1800 to –1800 r/min. The healthy three-phase system finished the reversal rotation in 0.6 s. After the fault, the loss of one-phase leads to roughly the $1/\sqrt{3}$ times of maximum torque output derating under the same current magnitude; hence, the two-phase system needs more time (nearly 1.1 s) to follow the reference speed, as shown in Fig. 13. From the perspective of faulty system, the dynamic response performance in transient condition is still satisfying, without the need to adjust PI parameters.

To demonstrate the response of the proposed FTC method under transient load changes, the load test is conducted at 1800 r/min in Fig. 14. Restricted by the maximum current magnitude, the load torque is lower than the rated torque. When the load torque steps, i_{qp} is transiently increased to keep the motor speed consistent with the reference speed, whereas the *d*-axis current is not affected to ensure the rotor flux stable. Whether it is in healthy or faulty conditions, the current response to the same load disturb is approximative due to unaffected voltage utilization. Under no-load situation, the current qualities in the two modes are all with low distortion. After the load steps up, high-frequency harmonics can be captured from two conditions. No obvious current imbalance can be detected even after the fault, showing satisfying current component control performance.

In this section, the dynamic performance of the postfault system is tested. By comparing with the response of the healthy system under the same working conditions, it is proved that the faulty system under proposed FTC still has relatively excellent operation capability.

C. Maximum Linear Speed Range Comparison

To explore the postfault voltage utilization variation, and quantify the expansion of the linear speed range brought by the CMV injection, the voltage utilization comparison test is executed in Fig. 15. A total of four working conditions are compared: healthy system without CMV injection, healthy system with CMV injection, faulty system without CMV injection, and faulty system with CMV injection. The motor speed is fixed at 3000 r/min with identical flux and torque current. It can be seen that no current fluctuations can be found when the CMV is injected. The lower the p-p value of modulation waves, the greater the voltage utilization. Hence, the CMV injection can effectively improve the voltage utilization whether in the healthy or faulty condition through reduced modulation wave magnitudes. For the healthy system, the CMV injection help reduce the magnitude of modulation waves from 0.81 to 0.69 p.u., and the magnitude decreases from 0.89 to 0.79 p.u. under faulty condition.

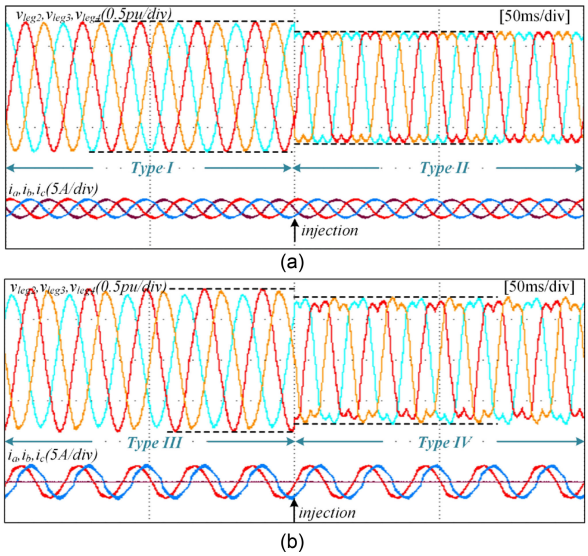

Fig. 15. CMV injection comparison. (a) Healthy condition. (b) Faulty condition.

TABLE III
VOLTAGE UTILIZATION COMPARISON UNDER DIFFERENT SITUATIONS

State	Healthy		Faulty			
Fault type	Type I	Type II	Type III	Type IV	Refs. [19]	Ref [24]
Utilization	0.87	1.00	0.79	0.89	0.29	0.50

By comparing the magnitude values of four situations (named Types I–IV in Fig. 15) and taking the case of healthy system with CMV injection (Type II) as unit one, the comparison results are given in Table II. For healthy system, the effect of CMV injection is equivalent to the SVPWM, and the 15% promotion of the voltage utilization is same as the theory. After the fault, the voltage utilization drops about 8% due to the modulation wave imbalance caused by negative-sequence suppression.

The voltage utilization results of existing FTC methods [19], [24] under the same postfault drive topology are also given in Table III. Obviously, the motor cannot continue to run at original speed when the postfault voltage utilization is less than 0.5 p.u. through existing methods. In contrast, the proposed method has better voltage utilization (0.89 p.u.) of it, due to the reasonable control setting and topology structure.

Moreover, to intuitively compare the methods described in the introduction and the proposal in several key fault-tolerant performance indexes, a radar map is given in Fig. 16.

We select the two most representative three-phase FTC solutions to compare with proposed ones. The work in [24] completes the FTC of 3+1 bridge topology, and the work in [19] achieves the FTC of full bridge by hardware reconfiguration. We can easily conclude that the proposed FTC method for series-end winding topology can achieve satisfying performance at a relatively low cost. Compared with the full-bridge topology with the most comprehensive fault-tolerant capability, the performance deficiency that is mainly reflected in the second category fault is acceptable, which shows excellent cost-effective features of SWMD.

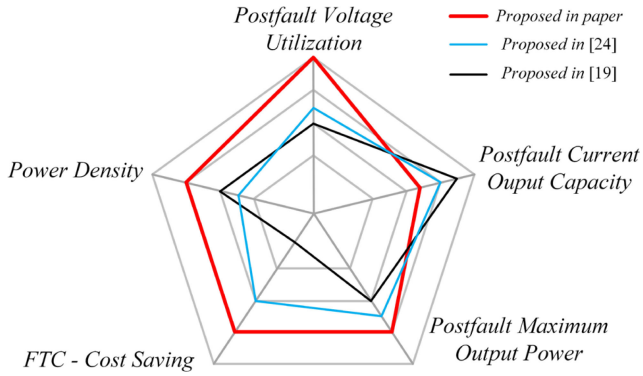

Fig. 16. Performance comparison between the proposed three-phase system and the others in introduction.

VI. CONCLUSION

Novel SWMD has been developed to expand the modulation index and speed range of the ac motor. In this article, a comprehensive fault condition analysis is given. Through the analytical results based on postfault asymmetrical structures, a simplified and practical FTC method applied for the first category of fault is proposed for the three-phase SWMD under the open-circuit fault. On the basis of positive-sequence control, the negative-sequence controller is employed to effectively eliminate the fault-induced second-order torque pulsations. The proposed FTC method in faulty conditions can achieve 91% of the dc voltage utilization in healthy conditions. With improved CMV injection method, the postfault linear speed range is further effectively extended by more than 11%. Experiment results verify that the proposed FTC method possesses excellent steady-state and dynamic response performance.

In general, the three-phase SWMD topology has the good fault-tolerant ability. Combined with the proposed FTC method, the following advantages can be obtained.

1) Simplified and reliable fault-dynamic transition procedure when the fault occurs. Based on the proposed self-adaptive strategy, the FTC part is activated in both healthy and faulty conditions, the fastness and accuracy requirements for fault detection algorithms are saved.
2) Excellent speed operation range even after the fault. The advantage of high voltage utilization for SWMD is fully exploited with proposed control methods and improved CMV injection method. Compared with existing fault-tolerant solutions, the maximum linear speed range can be greatly increased.

According to the advantages above, the proposed self-adaptive method is expected to help SWMD to be applied in high reliability and wide-speed applications.

REFERENCES

[1] W. Cao, B. C. Mecrow, G. J. Atkinson, J. W. Bennettm, and D. J. Atkinson, "Overview of electric motor technologies used for more electric aircraft (MEA)," *IEEE Trans. Ind. Electron.*, vol. 59, no. 9, pp. 3523–3531, Sep. 2012.

[2] A. M. Naradhipa, S. Kim, D. Yang, S. Choi, I. Yeo, and Y. Lee, "Power density optimization of 700 kHz GaN-based auxiliary power module for electric vehicles," *IEEE Trans. Power Electron.*, vol. 36, no. 5, pp. 5610–5621, May 2021.
[3] X. Peng, Z. Liu, and D. Jiang, "A review of multiphase energy conversion in wind power generation," *Renewable Sustain. Energy Rev.*, vol. 147, Sep. 2021, Art. no. 111172.
[4] Z. Liu, Z. Zheng, Q. Wang, and Y. Li, "Enhanced rotor field-oriented control of multiphase induction machines based on symmetrical components theory," *IET Power Electron.*, vol. 12, no. 4, pp. 656–666, 2019.
[5] I. G. Prieto, M. J. Duran, P. Garcia-Entrambasaguas, and M. Bermudez, "Field-oriented control of multiphase drives with passive fault tolerance," *IEEE Trans. Ind. Electron.*, vol. 67, no. 9, pp. 7228–7238, Sep. 2020.
[6] C. Zhu, Z. Zeng, and R. Zhao, "Comprehensive analysis and reduction of torque ripples in three-phase four-switch inverter-fed PMSM drives using space vector pulse-width modulation," *IEEE Trans. Power Electron.*, vol. 32, no. 7, pp. 5411–5424, Jul. 2017.
[7] Y. Zuo, X. Zhu, X. Si, and C. H. T. Lee, "Fault-tolerant control for multiple open-leg faults in open-end winding permanent magnet synchronous motor system based on winding reconnection," *IEEE Trans. Power Electron.*, vol. 36, no. 5, pp. 6068–6078, May 2021.
[8] R. R. Errabelli and P. Mutschler, "Fault-tolerant voltage source inverter for permanent magnet drives," *IEEE Trans. Power Electron.*, vol. 27, no. 2, pp. 500–508, Feb. 2012.
[9] R. Wang, J. Zhao, and Y. Liu, "A comprehensive investigation of four-switch three-phase voltage source inverter based on double Fourier integral analysis," *IEEE Trans. Power Electron.*, vol. 26, no. 10, pp. 2774–2787, Oct. 2011.
[10] W. Hu, C. Ruan, H. Nian, and D. Sun, "Simplified modulation scheme for open-end winding PMSM system with common DC bus under open-phase fault based on circulating current suppression," *IEEE Trans. Power Electron.*, vol. 35, no. 1, pp. 10–14, Jan. 2020.
[11] M. Tousizadeh, H. S. Che, J. Selvaraj, N. A. Rahim, and B. Ooi, "Performance comparison of fault-tolerant three-phase induction motor drives considering current and voltage limits," *IEEE Trans. Ind. Electron.*, vol. 66, no. 4, pp. 2639–2648, Apr. 2019.
[12] M. Tousizadeh, H. S. Che, J. Selvaraj, N. A. Rahim, and B. Ooi, "Fault-tolerant field-oriented control of three-phase induction motor based on unified feedforward method," *IEEE Trans. Power Electron.*, vol. 34, no. 8, pp. 7172–7183, Aug. 2019.
[13] A. Sayed-Ahmed, B. Mirafzal, and N. A. O. Demerdash, "Fault-tolerant technique for Δ-connected AC-motor drives," *IEEE Trans. Energy Convers.*, vol. 26, no. 2, pp. 646–653, Jun. 2011.
[14] A. Sayed-Ahmed and N. A. O. Demerdash, "Fault-tolerant operation of delta-connected scalar- and vector-controlled AC motor drives," *IEEE Trans. Power Electron.*, vol. 27, no. 6, pp. 3041–3049, Jun. 2012.
[15] A. Gaeta, G. Scelba, and A. Consoli, "Modeling and control of three-phase PMSMs under open-phase fault," *IEEE Trans. Ind. Appl.*, vol. 49, no. 1, pp. 74–83, Jan./Feb. 2013.
[16] H. T. Eickhoff, R. Seebacher, A. Muetze, and E. G. Strangas, "Post-fault operation strategy for single switch open-circuit faults in electric drives," *IEEE Trans. Ind. Appl.*, vol. 54, no. 3, pp. 2381–2391, May/Jun. 2018.
[17] A. Li, D. Jiang, W. Kong, and R. Qu, "Four-leg converter for reluctance machine with DC-biased sinusoidal winding current," *IEEE Trans. Power Electron.*, vol. 34, no. 5, pp. 4569–4580, May 2019.
[18] A. Li, D. Jiang, Z. Liu, and X. Sun, "Generalized PWM method for series-end winding motor drive," *IEEE Trans. Power Electron.*, vol. 36, no. 4, pp. 4452–4462, Apr. 2021.
[19] X. Zhang and C. Xu, "Second-time fault-tolerant topology and control strategy for the open-winding PMSM system based on shared bridge arm," *IEEE Trans. Power Electron.*, vol. 35, no. 11, pp. 12181–12193, Nov. 2020.
[20] A. Li, D. Jiang, X. Sun, and Z. Liu, "Online drive topology conversion technology for PMSM speed range extension," *IEEE Trans. Power Electron.*, vol. 37, no. 6, pp. 7113–7121, Jun. 2022.
[21] M. J. Duran, I. Gonzalez-Prieto, N. Rios-Garcia, and F. Barrero, "A simple, fast, and robust open-phase fault detection technique for six-phase induction motor drives," *IEEE Trans. Power Electron.*, vol. 33, no. 1, pp. 547–557, Jan. 2018.
[22] A. Arafat, S. Choi, and J. Baek, "Open-phase fault detection of a five-phase permanent magnet assisted synchronous reluctance motor based on symmetrical components theory," *IEEE Trans. Ind. Electron.*, vol. 64, no. 8, pp. 6465–6474, Aug. 2017.
[23] C. Sui, Y. He, Z. Li, and M. Chen, "The post-fault current model of voltage source converter and its application in fault diagnosis," *IEEE Trans. Power Electron.*, vol. 36, no. 2, pp. 1209–1214, Feb. 2021.
[24] H. Tang, W. Li, J. Li, H. Gao, Z. Wu, and X. Shen, "Calculation and analysis of the electromagnetic field and temperature field of the PMSM based on fault-tolerant control of four-leg inverters," *IEEE Trans. Energy Convers.*, vol. 35, no. 4, pp. 2141–2151, Dec. 2020.
[25] I. Jlassi and A. J. M. Cardoso, "Fault-tolerant back-to-back converter for direct-drive PMSG wind turbines using direct torque and power control techniques," *IEEE Trans. Power Electron.*, vol. 34, no. 11, pp. 11215–11227, Nov. 2019.
[26] M. Tousizadeh, H. S. Che, A. S. Abdel-Khalik, W. N. W. Munim, J. Selvaraj, and N. Abd Rahim, "Effects of flux derating methods on torque production of fault-tolerant polyphase induction drives," *IET Elect. Power Appl.*, vol. 15, no. 5, pp. 616–628, May 2021.
[27] X. Wang, Z. Wang, M. Gu, B. Wang, W. Wang, and M. Cheng, "Current optimization-based fault-tolerant control of standard three-phase PMSM drives," *IEEE Trans. Energy Convers.*, vol. 36, no. 2, pp. 1023–1035, Jun. 2021.
[28] F. Blaabjerg, D. O. Neacsu, and J. K. Pedersen, "Adaptive SVM to compensate dc-link voltage ripple for four-switch three-phase voltage-source inverters," *IEEE Trans. Power Electron.*, vol. 14, no. 4, pp. 743–752, Jul. 1999.
[29] J. Sun, Z. Zheng, C. Li, K. Wang, and Y. Li, "Optimal fault-tolerant control of multiphase drives under open-phase/open-switch faults based on DC current injection," *IEEE Trans. Power Electron.*, vol. 37, no. 5, pp. 5928–5936, May 2022.
[30] Y. Zhang, X. Pei, Z. Li, and P. Zhou, "Short-circuit current limiting control strategy for single-phase inverter based on adaptive reference feedforward and third harmonic elimination," *IEEE Trans. Power Electron.*, vol. 37, no. 5, pp. 5320–5332, May 2022.

Xiangwen Sun (Student Member, IEEE) was born in Hubei, China, in 1997. He received the B.S. degree in electrical engineering, in 2019, from Huazhong University of Science and Technology, Wuhan, China, where he is currently working toward the Ph.D. degree in electrical engineering with the School of Electronic and Electrical Engineering.

His research interests include inverter topology and control of multiphase machines.

Zicheng Liu (Member, IEEE) was born in Shandong, China, in 1989. He received the B.S. degree in hydropower engineering from Huazhong University of Science and Technology (HUST), Wuhan, China, in 2011, and the Ph.D. degree in electrical engineering from Tsinghua University, Beijing, China, in 2016.

From October 2014 to March 2015, he was a Visiting Student with Purdue University, West Lafayette, IN, USA. From June 2016 to September 2018, he was a Postdoc Researcher with Beijing Jiaotong University, Beijing, China. He is currently an Associate Professor with HUST. His research interests include multiphase motor control systems and transportation electrification.

An Li (Member, IEEE) was born in Wuhan, China, in 1996. He received the B.S. degree in electrical engineering, in 2017, from Huazhong University of Science and Technology, Wuhan, China, where he is currently working toward the Ph.D. degree in electrical engineering with the School of Electronic and Electrical Engineering.

His research interests include inverter topology, control strategy and modulation method for ac motor drive, reluctance motor drive, and multiphase motor drive.

Zhenyu Wang is currently working toward the M.S. degree in electrical engineering with the School of Electronic and Electrical Engineering, Huazhong University of Science and Technology, Wuhan, China, since 2019.

His research interests include ac motor drive, and control theory application in power electronics system.

Dong Jiang received the B.S. and M.S. degrees in electrical engineering from Tsinghua University, Beijing, China, in 2005 and 2007, respectively, and the Ph.D. degree in power electronics and motor drives from the University of Tennessee, Knoxville, TN, USA, in 2011.

From January 2012 to July 2015, he was with the United Technologies Research Center, East Hartford, CT, USA, as a Senior Research Scientist/Engineer. Since July 2015, he has been with Huazhong University of Science and Technology, Wuhan, China, as a Professor. His research interests include power electronics and motor drives, with more than 100 published IEEE journal and conference papers and more than 40 granted patents in these areas.

Dr. Jiang is an Associate Editor for the IEEE TRANSACTIONS ON INDUSTRY APPLICATIONS. He was the recipient of several Best Paper Awards in IEEE conferences.

Ronghai Qu (Fellow, IEEE) was born in China. He received the B.E.E. and M.S.E.E. degrees in electrical engineering from Tsinghua University, Beijing, China, in 1993 and 1996, respectively, and the Ph.D. degree in electrical engineering from the University of Wisconsin–Madison, Madison, WI, USA, in 2002.

Dr. Qu is a Full Member of Sigma Xi. He has been the recipient of several awards from the GE Global Research Center since 2003, including the Technical Achievement and Management Awards. He was also the recipient of the 2003 and 2005 Best Paper Awards, third prize, from the Electric Machines Committee of the IEEE Industry Applications Society (IAS) at the 2002 and 2004 IAS Annual Meeting, respectively.